

Section 4

**Parameterization of important
atmospheric and surface processes,
effects of different parameterizations**

An alternative method for handling the interactions between turbulence and phase changes

Jean-François Geleyn^{1,5}, Martin Vanandruel², Ivan Bašták-Řurán³, Daan Degrauwe⁴,
Filip Váňa⁵ & Radmila Brožková⁵

¹ CNRM, Météo-France, Toulouse, France – jean-francois.geleyn@meteo.fr

² Gent University, Ghent, Belgium

³ Comenius University, Bratislava, Slovakia

⁴ Royal Meteorological Institute, Brussels, Belgium

⁵ Czech Hydrometeorological Institute, Prague, Czech Republic

The problem of how to treat moist turbulence and the associated diffusive vertical transport of enthalpy and moisture under its three phases (or, equivalently, the ‘shallow convection’ issue) received a lot of attention over the past 40 years. Ideally one would like to extend without too much distortion the rather well calibrated methods of dry 1D vertical turbulent computation. Many algorithms have been proposed for that purpose, but most if not all of them, to our knowledge, rely on the Sommeria and Deardorff (1977) proposal and on the use of the so-called moist-conservative variables of Betts (1973). The procedure is then roughly as follows:

- Depending on the level of turbulent energy present in the grid-box, some assumptions are made about the PDFs of total water q_t and of liquid water potential temperature θ , both variables being assumed as ‘conservative’ in turbulent displacements with associated phase changes but without generation of precipitation.
- This statistical information allows: (i) to perform computations of the ‘resolved’ thermodynamic adjustment for the air parcel, with some cloud content C and some adjusted condensed water content q_c as by-products; (ii) with at least one additional hypothesis concerning the flux of q_c , to compute the grid-average turbulent buoyancy flux that will contribute to the time evolution of the Turbulent Kinetic Energy (TKE) and maybe of the Turbulent Potential Energy (TPE); (iii) to link, in fine via an equivalent cloud fraction N_{eb} , the turbulent fluxes of q_c and of potential temperature θ to those of q_t and of θ (in the most simple version of such schemes one somehow identifies N_{eb} to C).
- Once ‘(i)’ is performed and ‘(ii)’ has produced all the information (vertical exchange coefficients for momentum, heat and moisture, at least) needed to start the vertical diffusion calculations, the primary information given by water vapour q_v , plus q_c and θ is converted to the moist conservative variables, those are transported by diffusion and ‘(iii)’ allows to return to the evolution of the above-mentioned primary variables.
- It should be noted that this procedure amounts to do as if full evaporation takes place before an equivalent dry turbulent transport (but with condensation-modulated coefficients), followed by re-condensation at a rate determined by the analytical shape of the PDFs and by the link between N_{eb} and C .
- All the above remains true when considerations about third order correlations are added, allowing some part of the transport of enthalpy and/or moisture to become up-gradient.

In the course of this study we became aware of two limitations of the method just presented:

- The direct link between the ‘resolved’ thermodynamic adjustment and the treatment of the turbulent flux of q_c allows neither to use another method than the statistical one to determine C nor to distinguish between ‘stratiform’ and ‘convective’ origins for the average q_c present in the grid-box prior to the said adjustment. Precisely, within the framework of the so-called 3MT scheme for treating half resolved - half parameterised deep convection (Gerard et al., 2009), we would need such additional degrees of freedom.

- There is an intrinsic problem of vertical staggering: C is obtained by definition in the middle of the model layers while N_{eb} (monotonously depending on C) is required at their edges, i.e. where the fluxes of the prognostic variables are computed and combined. As long as the situation is relatively homogeneous in the vertical things are OK. But at cloud upper and lower edges, it is clear that mixing arbitrarily two radically differing non-linear behaviours will create numerical problems (and even probably physical ones).

To by-pass such obstacles, we propose a new procedure, based on the following three hypotheses:

- The ‘resolved’ thermodynamic adjustment procedure remains part of the ‘moist physics’ but its role is disconnected from that of vertical turbulent diffusive transport.
- This adjustment is best performed after the said transport has taken place in order to mix the advective and diffusive inputs to non-deep-convective condensation/evaporation processes.
- It is possible, from the sole ‘static’ knowledge of the state of the atmosphere at the beginning of the physics time-step, to compute a ‘shallow convective cloud cover’ C_{scv} at the interfaces between model layers. The latter quantity is such that a $(1 - C_{scv})$ vs. C_{scv} weighting of respectively ‘dry’ and ‘fully condensed’ buoyancy terms will deliver the input needed for the evolution of TKE (and maybe of TPE).

Of course the last of the three hypotheses is the most daring one of our proposal, but it is at the same time its anchor point. Since the ‘true’ value of C is yet unknown at the time when turbulent and diffusive computations are performed, a direct link between N_{eb} and C_{scv} (identity in the simplest case) can indeed exist without any vertical staggering problem. Moist buoyancy considerations for the conversion between TKE and TPE are thus directly related to the implicit hypotheses about where condensation/evaporation really takes place during the turbulent vertical transport of q_t , and this seems a sound basis for a physically true and numerically stable algorithm. Some additional remarks are however needed:

- For radiative computations, a preliminary estimate of C should be computed and combined with C_{scv} (as well as with some deep convective cloudiness). It is hoped that something like $C' = 1 - (1 - C^*)(1 - C_{scv})$ will rather closely anticipate the future value of C (with C^* the estimate based only on advection). This would be a point of verification of the integrity of the proposed scheme. Obviously the above-mentioned staggering problem has been displaced here (C^* vs. C_{scv}), but probably with less detrimental consequences.
- We left here fully open the actual ‘static’ analytical derivation of C_{scv} (or equivalently of the total buoyancy flux). What can be said at the present (early) stage of the study is that mimicking, via an analytical inversion, the situation of a heuristic enhancement of exchange coefficients (Geleyn, 1987) gives quite reasonable results. But we would obviously like to make a more ‘physical’ use of the independency granted in our proposal to the determination of C_{scv} .

Part of this work was performed in the framework of the EU-ESF COST ES0905 action or of the Czech GAAV Grant N° IAA300420804. Supports of the RC LACE Consortium as well as those of Météo-France and of Gent University are gratefully acknowledged.

References:

- Betts, A.K., 1973. *Quart. J. R. Met. Soc.*, **99**, pp. 178-196.
 Geleyn, J.-F., 1987. *J. Meteor. Soc. Japan, Special NWP Symposium Volume*, pp. 141-149.
 Gerard, L., J.-M. Piriou, R. Brožková, J.-F. Geleyn and D. Banciu, 2009. *Mon. Wea. Rev.*, **137**, pp. 3960-3977.
 Sommeria, G. and J.W. Deardorff, 1977. *J. Atmos. Sci.*, **34**, pp. 344-355.

Improvement of convection parameterization in high resolution limit

Luc Gerard*

(*) *Royal Meteorological Institute of Belgium, Luc.Gerard@oma.be*

In operational weather prediction models, the effect of subgrid phenomena on the large scale flow is usually evaluated with parameterizations. The resolved condensation is obtained from the mean grid-box conditions together with some hypotheses on the subgrid variability. To treat deep convection, that implies significant vertical transports, mass-flux schemes are very popular. They generally assume that the grid-boxes are sufficiently large to contain a wide variety of clouds at different stages of evolution, and that the fraction of the grid-box area occupied by these is small, so that the properties in the updraft area have small impact on the resolved properties. The scheme is closed by writing some steady-state diagnostics.

For grid-box length between 10 and 1km, used together with relatively short time-steps, these hypotheses are no longer satisfied. The resolved vertical velocity becomes significant, while the resolved condensation includes a significant part of the one associated to updrafts; it becomes difficult to combine fully separate contributions from the resolved and the updraft schemes. A common practice is then to suppress the convective parameterization, but the resolution is often not sufficient to completely resolve the convective cells at all stages of their evolution.

The relevant issues to improve parameterization include the time-evolution of the updraft vertical velocity, of the updraft horizontal extents and of its vertical extent (gradual raise of the cloud, while no steady-state is reached), and preventing concurrence between resolved and subgrid. In the point of view of modeling, the two first items can be handled by memorizing respectively an updraft velocity variable governed by a prognostic equation, and an updraft mesh fraction evolving at each time step. Both variables are advected by the mean flow. This technique was applied in the 3MT scheme [GERARD et al., 2009], together with a sequential organization of the parameterizations to make them complementary. The updraft condensation was combined with the resolved condensation before entering a single microphysics. This solution produced encouraging results down to 4km resolution, but the auto-extinction of the parameterization at higher resolution was not obtained.

In theory, using small grid-boxes implies that the mesh fraction could reach 100%; but in this case the construction of a buoyant subgrid updraft loses its pertinence, and in addition it is very difficult to get the subgrid contribution falling back to zero when all updrafts are resolved.

To get out of the deadlock, we developed a new scheme based on the concept of *virtual unresolved cloud*. It considers that physical updrafts can already be partly represented by the resolved motion and the resolved condensation scheme, and that parameterization should simply produce a complementary contribution to these.

We take as prognostic variable $\omega_u^\diamond = \omega_u - \bar{\omega}$, the difference between absolute updraft velocity ω_u and resolved vertical velocity $\bar{\omega}$. The subgrid mesh fraction σ_u represents the total fraction occupied by the updrafts only when the resolution is coarse and $\bar{\omega}$ is small. At high resolution, it is associated with a virtual updraft, complementing the resolved one. The virtual updraft condenses with $\sigma_u \omega_u^\diamond$, transports and entrains with $\sigma_u(\omega_u - \omega_e)$

where ω_e is the velocity in the grid-box updraft environment, and rises with the absolute velocity ω_u .

The virtual updraft is necessarily confined in a grid column. An upwards motion of the updraft parcel (wrt the mean grid-box motion) is compensated by a downwards motion of the dryer environment. Following e.g. ASAI and KASAHARA [1967], the subsiding motion is accompanied by a dry adiabatic heating reducing the net buoyancy. This effect is accounted for in our formulation, and depending of the vertical dry and moist lapse rates, the maximum consumption of energy by the subgrid updraft occurs for $\sigma_u = 0.4$ or less; subsequently σ_u will never be greater than this value.

The short time-steps make it necessary to allow a gradual rise of the updraft top; the vertical equation also accounts for the fraction of the time-step a given level is reached by the rising updraft. The mesh-fraction evolution is currently estimated with a diagnostic of the steady-state value (not reached) and an evolution equation towards it.

Preliminary tests at varying resolution in three-dimensional model show a significant decrease – though not a complete extinction – of the convective contribution when the mesh-size decreases from 8 to 1km. The figure below shows that the subgrid-scheme share remains important mainly for low total precipitation amounts. Additional refinements are studied to further improve the convergence towards explicit convection.

This research is done in the frame of the European-Community COST-ES0905 action.

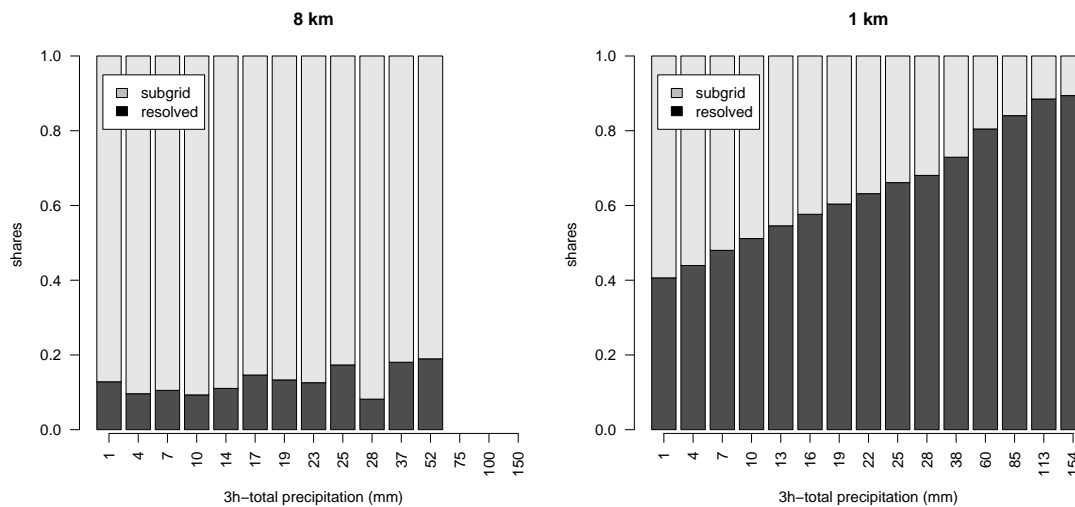


Figure 1 : Resolved and subgrid respective proportions for several classes of forecast surface precipitation intensities. Convective event over Belgium (10-09-2005). Left: 8km-, right: 1km-mesh-size

References

- T. ASAI and A. KASAHARA. A theoretical study of the compensating downward motions associated with cumulus clouds. *J. Atm. Sci.*, 24:487–496, September 1967.
- L. GERARD, J.-M. PIRIOU, R. BROŽKOVÁ, J.-F. GELEYN, and D. BANCIU. Cloud and precipitation parameterization in a meso-gamma scale operational weather prediction model. *Mon. Wea. Rev.*, 137:3960–3977, 2009.

Improvement of Kain-Fritsch Convection Parameterization Scheme To Suppress its False Predictions of Rainfall Areas along Coastal Lines

Teruyuki KATO¹, Yoshinori YAMADA¹ and Masuo NAKANO²

¹ Meteorological Research Institute/Japan Meteorological Agency, Tsukuba, Ibaraki, Japan

² Advanced Earth Science and Technology Organization, Tsukuba, Ibaraki, Japan

The operational mesoscale model (MSM) of the Japan Meteorological Agency (JMA) with a horizontal resolution of 5 km (Saito et al. 2007) often makes false predictions of rainfall areas along coastal lines, not observed, during warm season, especially in July and August (see Fig. 2a). Such a rainfall area is predicted due to the oversensitive activation of the Kain-Fritsch convection parameterization scheme (K-F scheme; Kain 2004) introduced in the MSM, when low-level humid air inflows from the sea into the land. The activation of the K-F scheme is judged by lifting the updraft source layer (USL) to the lifting condensation level (LCL) and checking the atmospheric conditions for the formation of moist convection. In the MSM, the temperature and water vapor in the USL are averaged in the layer with a depth of 50 hPa from the lowest vertical level of the model (~ 20 m). Narita (2008) introduced temperature perturbations based on the relative humidity into the K-F scheme to improve the predictions of the MSM, but the improvement can hardly suppress false predictions of rainfall areas along coastal lines.

At first, to improve the K-F scheme, the appearance frequency of cloud-base heights from the surface (CBHs) of moist convection, simulated by the 1km-cloud-resolving model (CRM), around Kyushu and Shikoku Islands (see Fig. 2a), western Japan during the 2008 warm season is statistically examined separately over the sea, around the coastal areas and in mountainous regions (heights > 500 m). The frequency in the ordinate of Fig. 1, normalized based on the maximum frequency, is for the case with an updraft exceeding the number (W_{max}) shown in the abscissa. Figure 1 also shows the appearance frequency of the W_{max} (bold curve). The case with an updraft exceeding 1.0 m s^{-1} appears at rates of 1.52 % ~ 4.64 %, while that exceeding 10.0 m s^{-1} decrease by more than two orders. However, the peak height of CBH appearance frequency changes a little for the increase of the W_{max} . The CBHs tend to appear higher around coastal areas than over the sea, and their appearance almost limits below a height of 200 m in mountainous regions.

The CBHs scarcely appear above a height of 1.0 km (1.5 km) over the sea (on the land) for $W_{max} > 5.0 \text{ m s}^{-1}$. This means that most of moist convection with strong updrafts has a considerably low CBH even on the land in East Asia during warm season, because the inflow of low-level humid air from the sea produces strong convection on the land. It should be noted that the extension of CBH appearance frequency to the upper level is found for weak W_{max} ($1 - 3 \text{ m s}^{-1}$). This extension could be brought from stratiform clouds.

As shown in Fig. 1, the appearance of CBH is remarkably different among sea, coast and mountain. In this study, the originating level to calculate the USL in the K-F scheme is changed based on the statistical examination of the CBHs. It should be noted that in the K-F scheme introduced into the JMA nonhydrostatic model (JMANHM) the originating level to calculate the USL can be set by a unit of 15 hPa from the lowest vertical level of the model (~ 20 m). In the improved K-F scheme, the originating level over

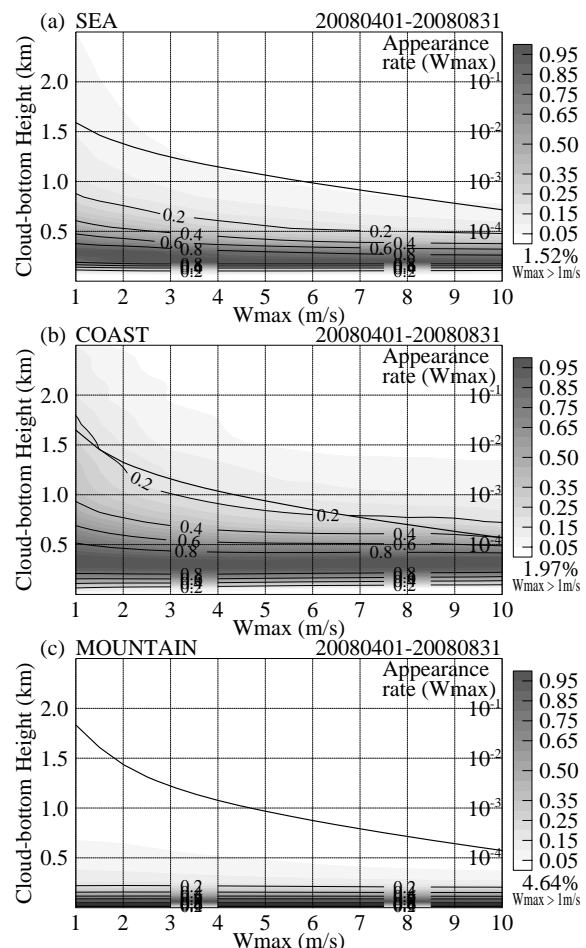


Fig. 1. Appearance frequency distributions of CBHs simulated by the 1km-CRM for maximum updrafts in vertical cores (a) over the sea, (b) around coastal areas and (c) in mountainous regions. The abscissa denotes the case with an updraft (m s^{-1}) exceeding the number (W_{max}), and the frequencies are normalized based on the maximum frequency in the ordinate. The bold curve shows the appearance frequency of W_{max} . The statistical period is the 2008 warm season between April and August.

the sea and in mountainous regions is set the lowest vertical level, while that around coastal areas is set 45 hPa (~ 500 m) above the lowest vertical level. The above-mentioned setting produces the discontinuity of the originating level. To avoid this discontinuity, the originating level in boundaries is set 15 hPa or 30 hPa above the lowest level of the model. A unit of 15 hPa is changed by two horizontal grids in this study.

Figure 2 shows the distribution of total rainfall amount in July 2006 simulated by the 5km-NHM. The 5km-NHM well reproduces the rainfall distribution, although it fails to simulate areas with total rainfall amount larger than 900 mm over the mountainous regions in the southern part of Kyushu Island. The 5km-NHM with the original K-F scheme (Fig. 2a) makes false predictions of rainfall areas along coastal lines (e.g., western part of Kyushu Island and south part of Shikoku Island). On the other hand, the 5km-NHM with the improved K-F scheme (Fig. 2b) hardly predicts such a rainfall area and the other rainfall distributions don't show a large difference from that with the original K-F scheme.

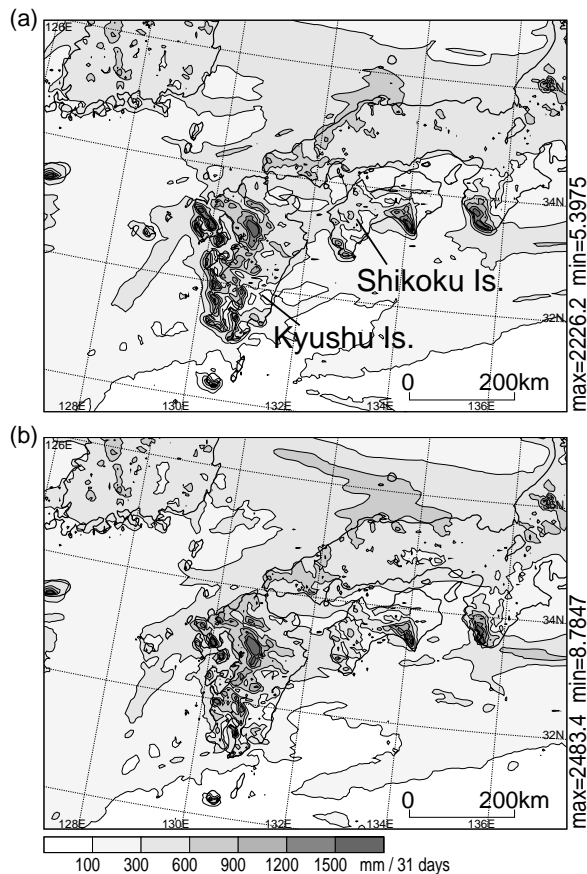


Fig. 2. Distribution of total rainfall amount in July 2006, simulated by the 5km-NHM with (a) the original and (b) improved K-F schemes.

Figure 3 shows the appearance frequency of hourly rainfall amounts in July 2006 observed by JMA raingauges (AMeDAS) and simulated by the 5km-NHM. The improved K-F scheme (thin curve) hardly changes the appearance frequency of rainfall amounts less than 15 mm, while it considerably reduces the underestimation of the 5km-NHM with the

original K-F scheme (dashed curve) for rainfall amounts larger than 15 mm. The cumulative appearance frequency (curves increasing to the right in Fig. 3) shows that the improved K-F scheme reduces the overestimation of the 5km-NHM with the original K-F scheme for rainfall intensity less than 15 mm. The appearance frequency of daily rainfall amounts (DRA) in July 2006 is also examined. The improved K-F scheme reduces the underestimation of the 5km-NHM with the original K-F scheme for 20 mm < DRA < 50 mm and its overestimation for 50 mm < DRA < 80 mm (not shown).

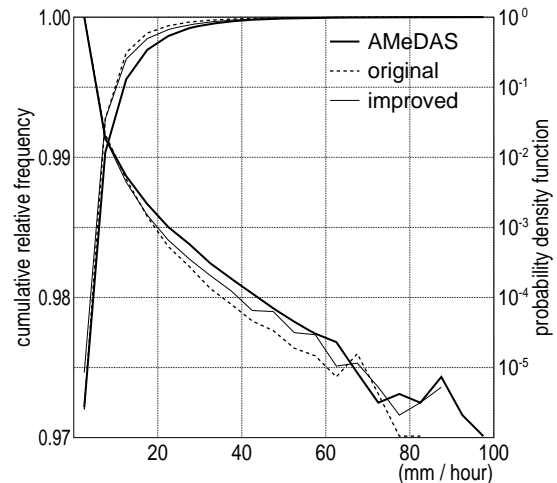


Fig. 3. Appearance frequency of hourly rainfall amounts in July 2006 observed by AMeDAS (bold curves) and simulated by the 5km-NHM with the original (dashed curves) and improved (thin curves) K-F schemes. The curves increasing to the right are the cumulative appearance frequency for the rainfall amounts exceeding the abscissa number, and its values are shown in the left ordinate. The curves decreasing to the right are the appearance frequency of hourly rainfall amounts, normalized based on that less than 5 mm h⁻¹.

In the case that the 5km-NHM is used to examine the change in future weather extremes, since such a false prediction due to the original K-F scheme produces some problems not to make quantitative statics for heavy rainfall amounts and floods, the improved K-F scheme can solve them. However, in this study, the improved K-F scheme is applied only to the 5km-NHM. Therefore, the application to NWP models with the other horizontal resolutions is needed. Moreover, the development of suitable convection parameterization schemes for global and mesoscale NWP models (e.g., the introduction of the level of free convection instead of the LCL in K-F scheme) must be continued to improve the accuracy of their predictions. These are in the future issues.

REFERECES

Kain, J. S., 2004: The Kain-Fritsch convective parameterization: An update. *J. Appl. Meteor.*, **43**, 170-181.
 Narita, M., 2008: Inclusion of a temperature perturbation based on the relative humidity to the Kain-Fritsch convective parameterization scheme. *CAS/JSC Research Activities in Atmospheric and Oceanic Modeling*, **39**, 4.11-4.12.
 Saito, K., J. Ishida, K. Aranami, T. Hara, T. Segawa, M. Nareta, and Y. Honda, 2007: Nonhydrostatic atmospheric models and operational development at JMA. *J. Meteor. Soc. Japan*, **85B**, 271-304.

Development of stochastic/ensemble neural network convection parameterizations for climate models using CRM simulated data

Vladimir Krasnopolsky, NOAA/NCEP and University of Maryland (UMD), Michael Fox-Rabinovitz, UMD, Philip Rasch DOE PNNL, Yefim Kogan, University of Oklahoma/UCSD-Scripps, Alexei Belochitski, UMD, and Peter Blossey, UW
Acknowledgements: Marat Khairoutdinov (SUNY – Stony Brook) for providing SAM

A novel approach based on the neural network (NN) technique has been formulated and used for development of NN stochastic/ensemble convection parameterizations for climate and NWP models. This fast NN convection parameterization is built based on direct learning cloud physics from CRM (Cloud Resolving Model)/SAM (System for Atmospheric Modeling, Khairoutdinov and Randall, 2003) simulated data. SAM/CRM simulations have been initialized with and driven/forced by 120-day long TOGA-COARE data. SAM/CRM simulated data have been averaged to produce hourly and horizontally, 256 km x 256 km, means. The data was projected onto a GCM space of atmospheric states to implicitly define a stochastic convection parameterization. Here NN serves as an interface transferring information about sub-grid scale processes from fine-scale data or models (SAM/CRM) into GCM (up-scaling). Actually, the averaged SAM output is “projected” on the CAM space or in other words, only a subset of relevant SAM variables available in a climate model (NCAR CAM) is selected, resulting in creating an NN training data set. The developed NNs have been trained and tested (i.e., their accuracy is estimated vs. SAM simulated data). The first 96 days of SAM simulated data are used for NN training, and the last 24 days for validation/testing, i.e., testing is done on an independent data set.

Different developed NN architectures use temperature and moisture vertical profiles as inputs and Q1C – the “apparent heat source”, Q2 – the “apparent moist sink” and cloudiness (CLD) vertical profiles as well as total precipitation as outputs. Some of the NN architectures also use vertical velocity and radiative heating rates profiles as additional inputs. The stochastic NN convection parameterization is defined by an ensemble of NNs with different architectures. The inherent uncertainty of the stochastic convection parameterization is indicated and estimated.

The accuracy of NN convection parameterization or similarity of time series of cloudiness and precipitation to SAM simulated data, is illustrated in Figs. 1 and 2.

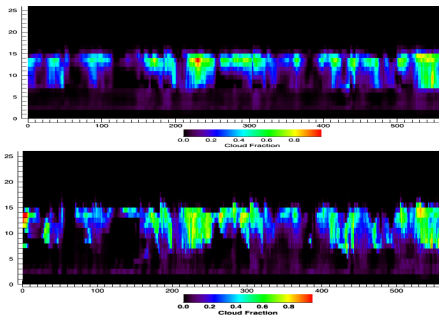


Fig. 1 Hovmöller diagrams for CLD profile (in fractions) time series; top - independent test data, bottom – NN convection.

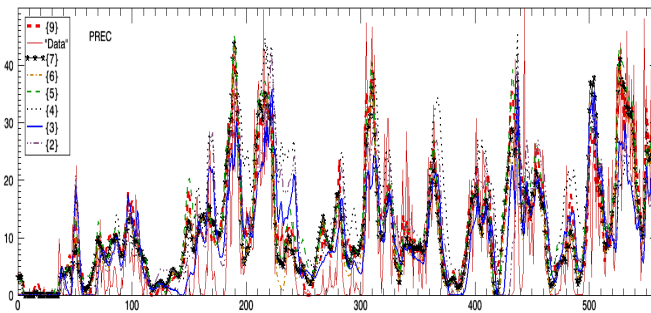


Fig. 2 Precipitation (in mm/day) time series for different NN architectures ($\{2\}$ - $\{9\}$) vs. independent test data (“Data”).

An initial validation of NN convection in NCAR CAM has been done in an off-line/diagnostic mode. Actually, CAM inputs have been used, at every time step of the control/original CAM integration, for parallel (off-line) calculations of the NN convection parameterization (CAM-NN) to produce its outputs as a diagnostic byproduct.

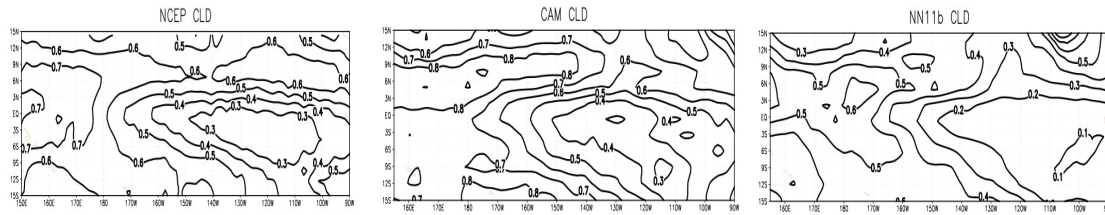


Fig. 3 Total CLD (in fractions, the contour interval is 0.1) for the Eastern Tropical Pacific Ocean (15 S to 15 N, 150 E to 90 W) for the 4-month TOGA-COARE period (Nov.-92 – Feb.-93) for the: NCEP reanalysis (left), control CAM (middle), and CAM-NN (right).

The CLD patterns shown in Fig. 3 are similar; their further in-depth analysis is needed. Note that the time series of precipitation and CLD for the CAM-NN- and control CAM runs (not shown) are similar in terms of both magnitude and frequency.

Conclusions

The presented initial results show the possibility of development of NN convection parameterizations based on learning cloud physics from CRM/SAM simulated data.

1. A novel approach based on using NNs is formulated and used for development of NN ensemble/stochastic convection parameterizations for climate models.
2. SAM/CRM simulations initialized with and driven/forced by TOGA-COARE data have been temporally and horizontally averaged and projected onto the GCM space of atmospheric states and used to derive very fast NN convection parameterizations with different architectures, and their accuracy is estimated.
3. Developed NN convection parameterizations have been validated in an off-line/diagnostic CAM (CAM-NN) run vs. the control CAM run. The initial results are encouraging: Total precipitation and cloudiness time series and tropical distributions for CAM-NN and CAM are realistic and consistent.
4. The NN convection parameterization can be applied to NWP models as well.

Future plans

1. Using long (3-year) ARM SGP data for driving SAM/CRM simulations for further developing and testing/validating NN convection parameterizations for mid-latitudes.
2. Using SAM/CRM simulations driven by CAM forcing for longer times, more geographic locations, and more diverse weather conditions so that NNs can be used globally and for all seasons, and validation of NN convection in CAM.

References

- Khairoutdinov, M., and D. Randall, 2003: Cloud resolving modeling of the ARM summer 1997 IOP: Model formulation, results, uncertainties, and sensitivities. *J. Atmos. Sci.*, **60**, 607–625.
- Krasnopolsky, V., M. Fox-Rabinovitz, Y. Kogan, A. Belochitski, and P. Blossey, 2010: Development of neural network convection parameterizations for climate models using Cloud Resolving Model simulations, NCEP Tech. Note, in preparation.
- Krasnopolsky, V., M. Fox-Rabinovitz, P. Rasch, Y. Kogan, A. Belochitski, and P. Blossey, 2010: Neural network convection parameterizations for climate models based on statistical learning from Cloud Resolving Model simulations, paper in preparation.

Modification to the mixing rate of a convective cloud in the Kain-Fritsch scheme

Masami Narita

Numerical Prediction Division, Japan Meteorological Agency

1-3-4 Otemachi, Chiyoda-ku, Tokyo 100-8122, Japan

E-mail: m_narita@naps.kishou.go.jp

To represent the effects of subgrid-scale convection, the Kain-Fritsch (KF) convective parameterization scheme (Kain and Fritsch, 1990; Kain, 2004) is adopted simultaneously with a cloud microphysics scheme to the Japan Meteorological Agency mesoscale model (MSM) of 5-km grid spacing. The KF scheme utilizes a one-dimensional entraining/detraining plume model and the mixing rate δM_e at which environmental air mixes into an updraft over a pressure interval δp is expressed as

$$\delta M_e = M_{u0} \left(\frac{-0.03 \delta p}{R} \right), \quad (1)$$

where R and M_{u0} are the updraft radius and the updraft mass flux at cloud base, respectively (Kain and Fritsch, 1990). In the current KF scheme, R varies between 1000 m and 2000 m based on the vertical velocity at the lifting condensation level (Kain, 2004).

According to Fig. 1, strong and deep convection near a typhoon center is represented mainly by cloud microphysics scheme. On the other hand, contribution of the KF scheme to precipitation is mainly distributed over the area with relatively weak precipitation, where the large scale forcing is weak and the height of cloud top is low. It is suggested that MSM of 5-km grid spacing can explicitly treat the large scale deep convection, while it still needs the parameterization for relatively small convective clouds. Considering that the original KF scheme was successfully developed in the model of grid spacing $\Delta x_0 = 25$ km and smaller convective clouds in more stable

area mix more with their environment (Cohen, 2000), R in Eq. (1) is modified as $kR\Delta x/\Delta x_0$, where k is a parameter and Δx is the grid spacing of MSM.

Figure 2 shows the results of precipitation by the MSM forecast with the original and modified KF scheme and that by the observation. Compared with the observation (a), too excessive orographic precipitation along the western coast of the Kyushu Island is calculated (b). This unnatural precipitation is the weak point of the current KF scheme in the MSM. On the other hand, as shown in Fig. 2 (c), (d), and (e), enlargement of the mixing rate δM_e by making k smaller eliminates this weak point. Vertical profile of heating rate above the western part of the Kyushu Island due to moist processes of the modified KF scheme in

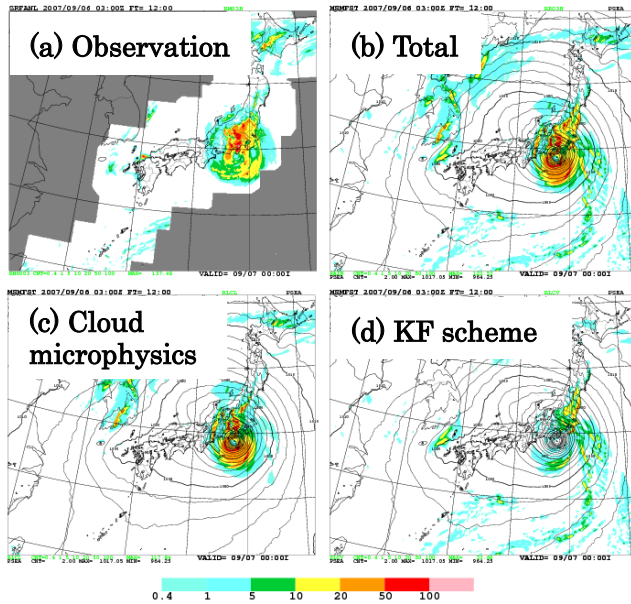


Fig. 1. Accumulated precipitation [mm/3h] at 15 UTC on September 7, 2007.

(a) Observation, (b) Contribution of cloud microphysics and the KF scheme, (c) Contribution of cloud microphysics, (d) Contribution of the KF scheme.

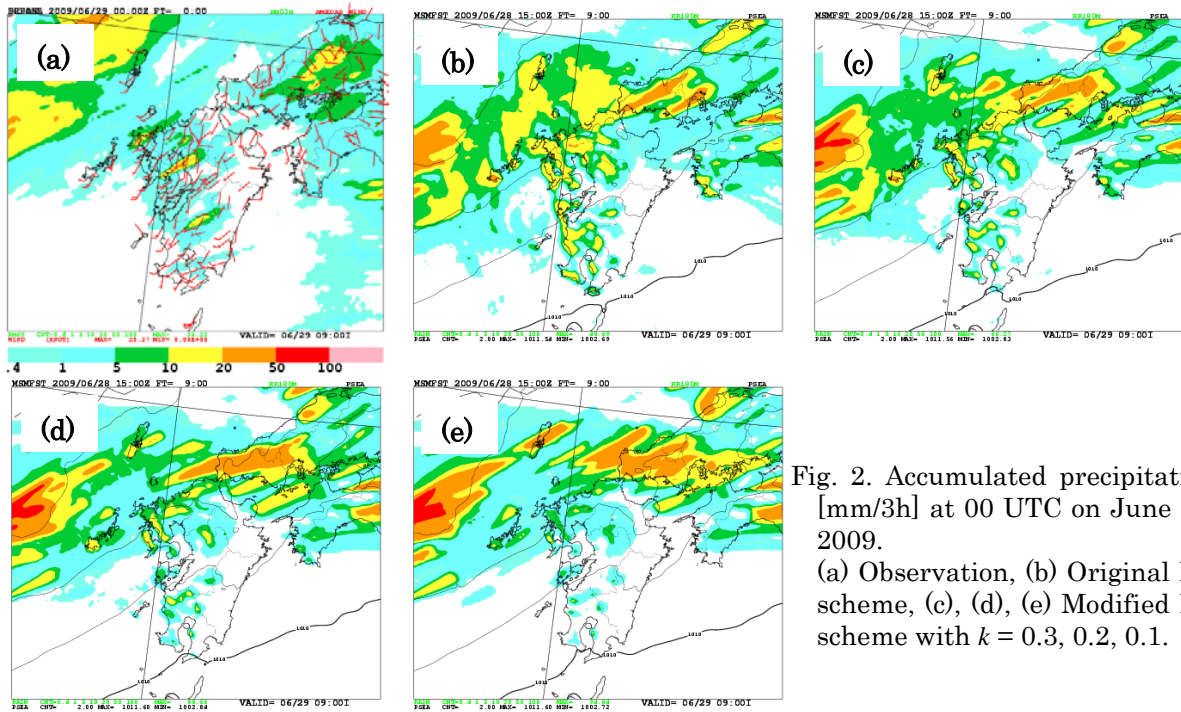


Fig. 2. Accumulated precipitation [mm/3h] at 00 UTC on June 29, 2009. (a) Observation, (b) Original KF scheme, (c), (d), (e) Modified KF scheme with $k = 0.3, 0.2, 0.1$.

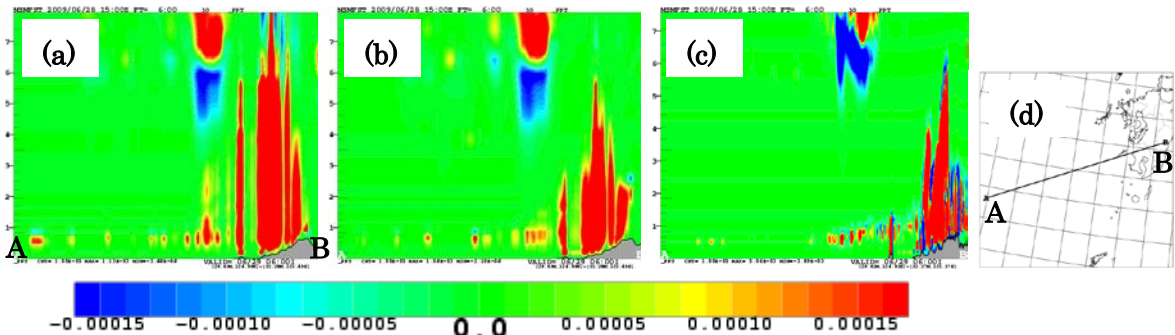


Fig. 3. Vertical profiles of heating rate [K/s] due to moist processes at 21 UTC on June 28, 2009. (a) Original KF scheme, (b) Modified KF scheme, (c) 1-km model with only cloud microphysics, (d) Locations of A and B.

the MSM becomes closer to that by a high resolution (grid spacing is 1 km) model without convective parameterization (Fig. 3). These results show the modification of the mixing rate in the KF scheme improves the forecasts of precipitation and heating rate by convection.

Further investigation such as the inclusion of variable mixing rate of convective clouds according to the height of cloud base has been continued.

References

Cohen, C., 2000: A quantitative investigation of entrainment and detrainment in numerically simulated cumulonimbus clouds. *J. Atmos. Sci.*, **57**, 1657-1674.

Kain, J. S., 2004: The Kain-Fritsch convective parameterization: An update. *J. Appl. Meteor.*, **43**, 170-181.

Kain, J. S., and J. M. Fritsch, 1990: A one-dimensional entraining/detraining plume model and its application in convective parameterization. *J. Atmos. Sci.*, **47**, 2784-2802.

Improved numerical solution of three-dimensional turbulence closure equations

V. Shnaydman

Department of Environmental Sciences, New Jersey State University-Rutgers, USA

Email: volff@envsci.rutgers.edu

The results of application the atmospheric boundary layer (ABL) model /1/ in Hydro-meteorological Center (Moscow) operational prediction system /2/ revealed the effectiveness of ABL modeling if the tidy coefficients were taken suitable for use /3/.

The approach developed /4/ allowed to get the numerical integration scheme of two-equation turbulence closure for the non-stationary, one-dimensional ABL without using the tidy coefficients. The improvement and application the numerical integration scheme to the three-dimensional ABL is given in this report

The turbulent kinetic energy (TKE) and dissipation equations of three-dimensional closure scheme includes the variable sign terms of horizontal advection A, buoyancy (B) and diffusion (D) and constant sign terms of the production and dissipation. The time integration scheme is used along with the method of successive approximations.

The linear and finite-difference forms of these equations are constructed in such a way that the criteria of stability and positive numerical solution are fulfilled. It is getting in such way. The terms

$A_i = \{ A, B, D \}, i = 1, 2, 3$ are written as

$$A_i = \delta_i A_i + (1 - \delta_i) A_i \quad \text{where } \delta_i = \begin{cases} 1 & A_i \geq 0 \\ 0 & A_i < 0 \end{cases}$$

The TKE (E) and dissipation (ε) equations are represented

$$\begin{aligned} \frac{\partial E}{\partial t} + \delta_1 A(E) + \delta_2 B + \delta_3 D(E) = \\ - (1 - \delta_1) A(E) - (1 - \delta_2) B - (1 - \delta_3) D(E) - \alpha_\varepsilon \frac{E^2}{K} + P \end{aligned} \quad (1)$$

$$\begin{aligned} \frac{\partial \varepsilon}{\partial t} + \delta_1 A(\varepsilon) + \delta_2 \frac{\varepsilon}{E} B + \delta_3 D(\varepsilon) = \\ - (1 - \delta_1) A(\varepsilon) - (1 - \delta_2) \frac{\varepsilon}{E} B - (1 - \delta_3) D(\varepsilon) + \frac{\varepsilon}{E} P - \frac{\varepsilon^2}{E} \end{aligned} \quad (2)$$

The forward-differencing scheme for integration in time and the linearization of square functions $\psi^2 = \{ E^2, \varepsilon^2 \}$ with the expressions $\psi^2 = 2\psi^{n+1}\psi^n - (\psi^n)^2$ transform the TKE equation (1).

$$\begin{aligned} E^{n+1}(t + \Delta t) + \\ \frac{E^{n+1}(t + \Delta t)}{E^n(t + \Delta t)} \times \Delta t \sum_{i=1}^4 \delta_i A_i^n(t + \Delta t) + 2\Delta t \times E^{n+1}(t + \Delta t) \frac{E^n(t + \Delta t)}{K^n(t + \Delta t)} = \\ - \Delta t \times \sum_{i=1}^4 (1 - \delta_i) A_i^n(t + \Delta t) + \Delta t (\alpha_\varepsilon \frac{(E^n(t + \Delta t))^2}{K^n(t + \Delta t)} + P^n(t + \Delta t)) + E(t) \end{aligned} \quad (3)$$

The integration in time is realized in such way.

$$\begin{aligned}
E^{n+1}(t + \Delta t) = & (-\Delta t \times \sum_{i=1}^4 (1 - \delta_i) A_i^n(t + \Delta t) + \\
& \alpha_\varepsilon \Delta t \frac{(E^n(t + \Delta t))^2}{K^n(t + \Delta t)} + \Delta t P^n(t + \Delta t) + E^n(t)) \times \\
& (1 + \frac{\Delta t}{E^n(t + \Delta t)} \sum_{i=1}^4 \delta_i A_i^n(t + \Delta t) + 2\alpha_\varepsilon \Delta t \frac{E^n(t + \Delta t)}{K^n(t + \Delta t)})^{-1}
\end{aligned} \tag{4}$$

The same procedure is fulfilled for the dissipation equation (2).

$$\begin{aligned}
\varepsilon^{n+1}(t + \Delta t) = & (-\Delta t \times ((1 - \delta_1) A_1^n(t + \Delta t) + (1 - \delta_3) A_3^n(t + \Delta t) + \\
& \frac{\varepsilon^n(t + \Delta t)}{E^n(t + \Delta t)} ((1 - \delta_2) A_2^n(t + \Delta t) - P^n(t + \Delta t)) + \\
& (1 - \delta_3) A_3^n(t + \Delta t)) + \Delta t \alpha_\varepsilon \frac{(\varepsilon^n(t + \Delta t))^2}{E^n(t + \Delta t)} + \varepsilon^n(t)) \times \\
& (1 + \frac{\Delta t}{\varepsilon^n(t + \delta t)} (\delta_1 A_1^n(t + \Delta t) + \delta_3 A_3^n(t + \Delta t) + \\
& \delta_3 A_3^n(t + \Delta t)) + 2\alpha_\varepsilon \Delta t \frac{\varepsilon^n(t + \Delta t)}{E^n(t + \Delta t)} + \\
& \frac{\Delta t}{E^n(t + \delta t)} \delta_2 A_2^n(t + \Delta t))^{-1}
\end{aligned} \tag{5}$$

The quantities $E^{n+1}(t + \Delta t)$, $\varepsilon^{n+1}(t + \Delta t)$ and $E^n(t + \Delta t)$, $\varepsilon^n(t + \Delta t)$ in the expressions (3-5) are the variables of the next and previous iterations at the prediction instance of time, $E^n(t)$, $\varepsilon^n(t)$ are the variables at the initial instance of time period $t, t + \Delta t$. All terms in these expressions are positive and it provides the positive solution of the turbulence parameters automatically.

1. Shnaydman V, Berkovich L, Tarnopolskiy A (1997) Hydrodynamic model of the atmospheric and oceanic boundary layers. Russian Meteorology and Hydrology 7, 40-52
2. Shnaydman V., Berkovich L. (2006) Atmospheric boundary layer modeling in numerical prediction operations. Research Activity in Atmospheric and Oceanic Modeling #36, 5-57
3. Shnaydman V., Stenchikov G., Berkovich L. (2007) Advanced model of atmospheric boundary layer. Research Activity in Atmospheric and Oceanic Modeling #37, 5-33
4. Shnaydman V. (2009) Numerical integration of two-equation turbulence closure scheme. Research Activity in Atmospheric and Oceanic Modeling #39, 4-15

Development of Land-surface Processes in the JMA Nonhydrostatic Model

Masashi Ujiie¹ and Daisuke Miura²

¹*Numerical Prediction Division, Japan Meteorological Agency*

²*Office of Marine Prediction, Japan Meteorological Agency*

1-3-4 Otemachi, Chiyoda-ku, Tokyo 100-8122, Japan

E-mail: ujiie@met.kishou.go.jp

1 Introduction

At the Japan Meteorological Agency, mesoscale model (MSM) output is used as input data for applications such as maximum/minimum temperature forecasts and weather classifications. Land surface processes of NWP models play roles of lower boundary conditions and influence atmospheric conditions near the surface. Accordingly, surface process improvement is an important task in the development of the MSM.

The operational MSM employs a simple slab model as a land surface scheme, in which the effects of vegetation are expressed only as the influence of stomatal resistance on the computation of latent heat flux. The initial conditions of soil moisture are set to climatological values. Snow is expressed as a kind of land use, and the conditions of land use are constant during the time integration of the model. Because of this simplification, the MSM sometimes fails to forecast surface air temperature accurately, underestimating the maximum temperature on hot days and the minimum temperature on snow melting days.

The JMA nonhydrostatic model, the forecast model of the MSM, includes a more detailed land surface model called the MJ-SiB (MRI/JMA Simple Biosphere model) as an option. We are developing the MJ-SiB for implementation into the operational MSM, and this report focuses on recent improvements to the MJ-SiB.

2 Specifications of the MJ-SiB

The MJ-SiB is based on the New-SiB (Hirai et al. 2007) implemented into JMA's Global Spectral Model. The MJ-SiB includes three models, a vegetation canopy model, a soil model and a snow model. The vegetation canopy model (hereafter, canopy model) is based on Sellers et al.(1986), and considers evaporation and transpiration from canopy and grass cover. The canopy model is directly coupled with the atmospheric model. The soil model has three and four layers for soil moisture and temperature, respectively. Diffusive equations are solved to forecast soil temperature and the saturation rate of soil moisture and phase changes in soil moisture are considered in the model. The snow model employs a multiple layer structure (four layers at maximum) with the number of layers depending on the amount of snow wa-

ter equivalent amount.

3 Categories of vegetation types

For the original MJ-SiB, distribution of vegetation is divided into 13 categories (Dorman and Sellers, 1989). To allow the use of data with higher resolution and accuracy for the Japan Area, We add 12 further categories of vegetation based on land use data produced by the country's Geographical Survey Institute. The new categories are forest, farmland, urban area, each of which is subdivided into four smaller categories according to the coverage rates of forest or buildings in individual grids. Parameters such as the Leaf Area Index and coverage rate of the vegetation are set in each new category.

4 Improvement of computational stability

Figure 1 shows a time series of temperature forecasted/diagnosed by the canopy model. The curves of temperature oscillate with a frequency of $2\Delta t$. In particular, T_1 (the temperature at the lowest level of the atmospheric model) and T_c (the temperature at the canopy) reach $270K$ because of this oscillation. The oscillation is due to the computational instability.

To solve the problem, we refined the prognostic equations of the canopy model. First, an implicit scheme is employed for the eddy diffusive term of the equation for T_1 . Then, we evaluate the eddy diffusive term for heat based on the vertical gradient of dry static energy replacing vertical gradient of temperature. Finally, the future values of T_a and Q_a (canopy air temperature and water vapor) are returned to the atmospheric model. All of these modifications reduce the magnitude of surface and turbulent fluxes, and stabilize the time integration. Figure 2 shows a time series of temperature in a case with the modified MJ-SiB. The modifications remove almost all the oscillation and make the time integration stable. Due to the reduction of turbulent fluxes to the upper atmosphere, the temperature in the canopy model becomes higher than that shown in Figure 1.

5 Performance of the MSM coupled with the MJ-SiB in summer

To assess the performance of the MSM coupled with the MJ-SiB, a number of experiments were carried out for summer conditions. In this section, we outline an experiment for a period of heavy rain (3 to 7 August 2008). Hereafter, we refer to the experiments using the MJ-SiB and operational surface scheme as SiB and Rtn, respectively. Figure 3 shows the mean errors (ME) for surface air temperature of each experiment in the period of heavy rain days. Compared to Rtn, SiB expands the negative and positive biases during the daytime at nighttime, respectively. The positive biases expand rapidly in the evening (6 to 9 UTC in Figure 3). This means that SiB damps the diurnal cycle of temperature near the surface. The amplitude of the diurnal cycle strongly depends on the heat capacity of the ground skin. Using an analogy of the force restore method (Deardorff, 1978), the heat capacity of the ground skin can be estimated as follows;

$$c_g = \sqrt{\frac{c_s \rho_s k_s}{2\omega}} \quad W / (m^2 \cdot K)$$

$c_s \rho_s$ and k_s represent the heat capacity per unit volume and the thermal conductivity of the soil. ω is equal to the angular frequency for a day. According to the values of $c_s \rho_s$ and k_s in Pielke(2002), c_g varies from $O(10^4) \sim O(10^5) W / (m^2 \cdot K)$. In the MJ-SiB, c_g is set to $2.5 \times 10^5 W / (m^2 \cdot K)$, at the high end of the range. When the heat capacity of the ground skin was reduced to one thirds of its original value, the ground skin temperature tended to fall in the evening. Positive biases in the evening were reduced (see the curve of SiBcap in Figure 3).

6 Summary and future plans

We have been developing the MJ-SiB for implementation into the operational MSM. Preparation of landuse data and the improvement of computational stability have been carried out over the last few years. Numerical experiments for the summer season showed that the performance of the MSM coupled with the MJ-SiB depended on the heat capacity of the ground skin in the evening. Reducing the heat capacity to within a realistic range, made the mean error of surface temperature comparable to that of the operational MSM.

It is important in short range forecasting to estimate the initial conditions of temperature, water and snow depth at the land surface. We are also developing a land-surface analysis system using the offline version of MJ-SiB. In this system, the land-surface model is driven by atmospheric forcing data such as analyzed temperature, wind, observation based precipitation, and sunlight. The

land surface analysis is expected to impact on forecasts of the MSM when the surface is too dry/wet or covered with snow.

References

- Deardorff, J. W., 1978: *J. Geophys. Res.*, **83**, 1889-1903
 Dorman, J. L. and P. J. Sellers, 1989: *J. Appl. Met.*, **28**, 833-855
 Hirai, M., 2007: *J. Meteor. Soc. Japan.*, **85A**, 1-24
 Sellers, P. J. et al., 1986: *J. Atmos. Sci.*, **43**, 505-531
 Pielke, R. A., 2002: *Mesoscale Meteorological Modeling*, Academic Press, 402pp

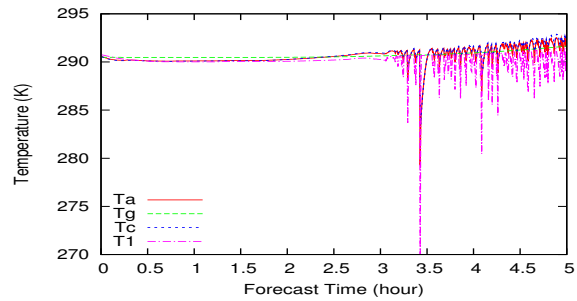


Figure 1: Time series of temperature of the canopy model. Ta:Air temperature in the canopy, Tg:Ground skin temperature Tc:Canopy Temperature T1:Air temperature at the lowest level of the atmospheric model.

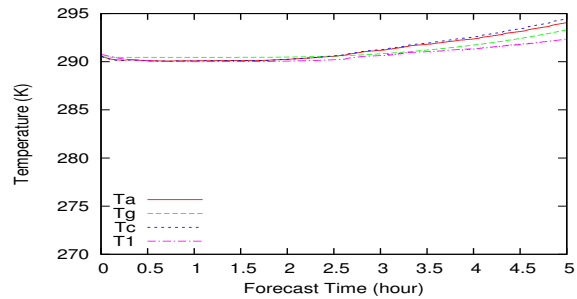


Figure 2: Same as Figure 1 but for the computationally stabilized MJ-SiB

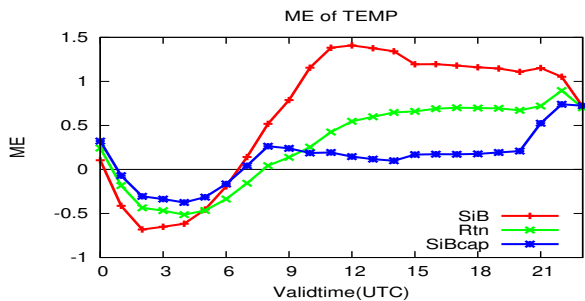


Figure 3: Time series of mean error of surface temperature.

Introduction of mire parameterization into numerical weather prediction model SL-AV

Alla Yurova¹, Mikhail Tolstykh^{2,1}

(1) Hydrometeorological Centre of Russia, Moscow, Russia

(2) Institute of Numerical Mathematics, Russian Academy of Sciences, Moscow, Russia

E-mail: alla.yurova@gmail.com

Including horizontal heterogeneity of soil moisture into the numerical weather prediction (NWP) model is one of the research priorities (e.g., Gedney and Cox, 2003). Mires change significantly the thermal regime and moisture status of the territory in the boreal zone where mires are numerous. Here we present a first attempt to develop a mire parameterization for the NWP model. SL-AV (semi-Lagrangian, absolute vorticity) is a 3D global finite-difference numerical weather prediction model (Tolstykh, 2001) used operationally in the Hydrometeorological Center of Russia. The current version of the model has the horizontal resolution of $0.9 \times 0.72^\circ$ lon-lat and 50 vertical levels. Mire parameterization consisted of the following model modifications:

- (1) force-restore method used to simulate soil temperature was replaced by the solution of the heat diffusion equation in the multilayer model domain (Wania et al., 2009), thermal properties of the peat were specified;
- (2) Mixed Mire Water and Heat model (MMWH, Granberg et al., 1999) was used to simulate the water table position, evapotranspiration, and runoff from a mire;
- (3) prescribe albedo, emissivity and roughness length for this type of ecosystems were used.

We used data on prescribed mire area extent (Vompersky et al., 2005) shown in Figure 1. The modified version of the NWP model SL-AV was used in online simulations for July-August 2008 starting from the initial conditions at 00 UTC.

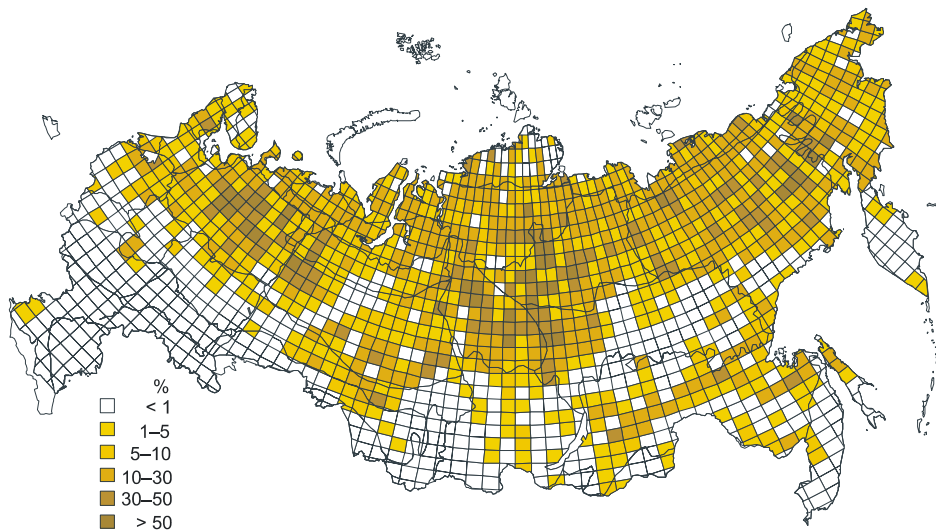


Figure 1. Map of the mire spatial distribution on the territory of Russia (Vomperskiy *et al.*, 2005)

The components of the energy balance were estimated for the mire grid cells in the area $60-85^\circ\text{E}$, $55-63^\circ\text{N}$ (Western Siberian Lowlands) where mires are abundant. The latent heat flux has increased strongly with the incorporation of evaporation from mires into the model. This increase

of the latent heat flux has produced a surface cooling. As a result, the sensible heat flux and outgoing terrestrial long-wave radiation decreased.

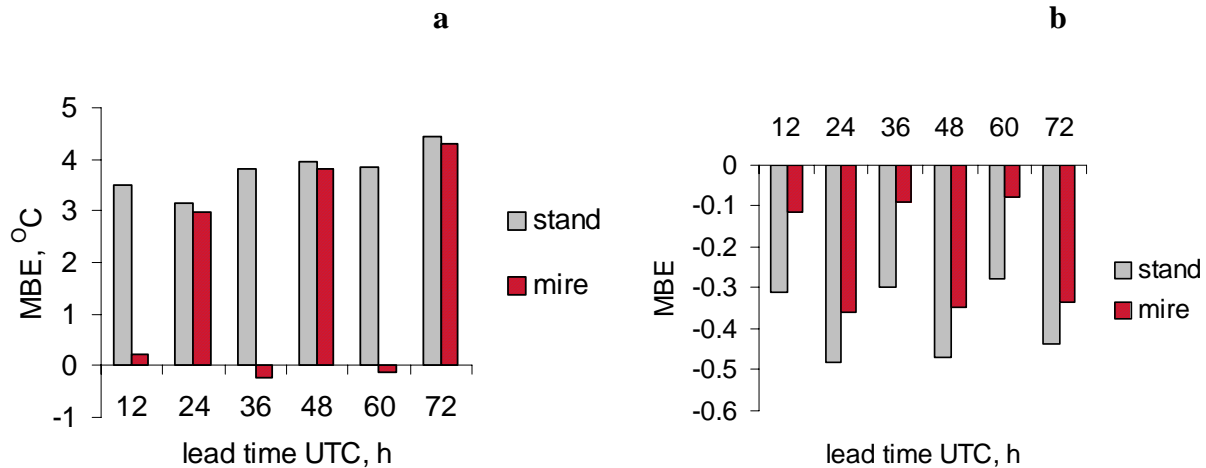


Figure 2. Mean bias error (MBE) for the standard run (stand) and run with included mire parameterization (mire): (a) 2-m temperature and (b) 2-m relative humidity.

Forecast skill was estimated using measurements at the meteorological stations in Western Siberia (60-85°E, 55-63°N) situated in the mire vicinity. Stations included in the analysis had at least 50% covered by mires in each of the 4 adjacent nodes. An error reduction is seen both in 2-m temperature and relative humidity (RH) forecast with lead times of 12, 36 and 60h starting at 00 UTC when mire parameterization was implemented (Fig. 2). Some improvement is seen in RH forecast with lead times of 24, 48 and 72h, but an error reduction in 2-m temperature is more modest at these time points (Fig. 2). Almost two times reduction is seen in root-mean-squared error of temperature and RH for lead times of 12, 36 and 60h, for example, RMS temperature error for 36 hours forecast is reduced from 4.8 to 5.9°C. Therefore, the mire parameterization helped to reduce a large warm temperature bias in the forecast for lead times of 12, 36 and 60h, but did not eliminate forecast bias for lead times of 24, 48 and 72h. We hypothesize that remaining errors in morning hours (local time) is due to model faults in the surface layer mixing dynamics.

References

- Gedney, N., and P. M. Cox (2003), The Sensitivity of Global Climate Model Simulations to the Representation of Soil Moisture Heterogeneity. *Journal of Hydrometeorology*, **4**, 1265-1275.
- Granberg, G., H. Grip, M. Ottosson-Lofvenius, I. Sundh, B. H. Svensson, and M. Nillsson (1999), A simple model for simulation of water content, soil frost, and soil temperatures in boreal mixed mires. *Water resources research*, **35**, 3771-3782.
- Tolstykh M.A. Semi-Lagrangian high-resolution atmospheric model for numerical weather prediction. *Russian Meteorology and Hydrology*. 2001, N 4. P. 1 - 9
- Vomperskij, S. J., A. A. Sirin, O. P. Cyganova, N. A. Valjaeva, and D. A. Majkov (2005), Bolota i zabolochennye zemli Rossii: popytka analiza prostranstvennogo raspredenenija i raznoobrazija. *Izvestiya RAN. Seriya geograficheskaya* **5**, 39-50 (in Russian).
- Wania, R., I. Ross, and I. C. Prentice (2009), Integrating peatlands and permafrost into a dynamic global vegetation model: 1. Evaluation and sensitivity of physical land surface processes. *Global Biogeochem. Cycles*, **23**, GB3014, doi:3010.1029/2008GB003412